IEEE Access
Multidisciplinary | Rapid Review | Open Access Journal

Received May 8, 2020, accepted May 27, 2020, date of publication June 1, 2020, date of current version June 11, 2020.

Digital Object Identifier 10.1109/ACCESS.2020.2998731

Sensorless Control of Segmented PMLSM for Long-Distance Auto-Transportation System Based on Parameter Calibration

TONG WEN[1,2], ZHONGYI WANG[1], BIAO XIANG[3], BANGCHENG HAN[1], (Member, IEEE), AND HAITAO LI[1], (Member, IEEE)

[1]School of Instrumentation and Optoelectronic Engineering, Beihang University, Beijing 100191, China
[2]Ningbo Institute of Technology, Beihang University, Ningbo 315000, China
[3]Department of Mechanical Engineering, The Hong Kong Polytechnical University, Hong Kong

Corresponding author: Biao Xiang (thomas.biao@gmail.com)

This work was supported in part by the Beijing Natural Science Foundation under Grant 3182024, and in part by the National Natural Science Foundation of China under Grant 61374211 and Grant 61773038.

ABSTRACT The permanent magnet linear synchronous motor (PMLSM) with segmented stator is applied in the long-distance auto-transportation system. For the PMLSM with the discontinuous stators, the mismatch between the permanent magnet (PM) mover and the stator would make electromagnetic (EM) parameters deflect nominal values, and then position/speed precision of the PM mover would be affected. In this article, the sensorless control based on the parameter calibration is used to drive the PM mover above the segmented stators during the drive process. Furthermore, an improved model reference adaptive integrator based on the parameter calibration is proposed to calibrate the EM parameters during the switch process. The simulation and experimental results confirm that the speed precision and the robustness of the segmented PMLSM are enhanced distinctly.

INDEX TERMS PMLSM, segmented stator, parameter calibration, sensorless control.

I. INTRODUCTION

The auto-transportation system is widely used in factory automation because of its advantages on fast response speed and great capacity. In general, the traditional auto-transportation system adopts the mechanical conversion system to transfer rotational motion into linear motion, but this kind of auto-transportation system could not satisfy requirements on rapidity, high efficiency, great load capacity and low energy consumption [1]. Therefore, the permanent magnet linear synchronous motor (PMLSM) is widely used in the auto-transportation system due to its advantages on high reliability, high motor efficiency and great power density [2]–[4]. However, the stators in the continuous PMLSM are usually continuously connected and arranged on the transportation rail, so the flexibility of the continuous PMLSM is weakened and the initial cost is increased in the long-distance auto-transportation system [5]. In order to solve this problem, a new structure of PMLSM with discontinuous stators is becoming the research focus of the long-distance auto-transportation system [4], [6]–[11].

For the purpose of reducing the high cost of sensors and improving the robust stability of the segmented PMLSM, the sensorless control method was proposed in the segmented PMLSM system [12]–[15]. The back electromotive force (EMF) integration method was often used in the sensorless control of the PMLSM [16], [17], but it exhibited poor estimation accuracy at low speed and had obvious integral drift. The sensorless control method based on the high-frequency signal injection was also studied [18], and it was applied to the stator winding by superimposing a high-frequency voltage on the fundamental wave signal. So, the position information was obtained through resolving the corresponding high-frequency current, and then the position signal could be achieved by the band-pass filter. However, this method had strict requirements on the saliency ratio of motor. Furthermore, the extended Kalman filter [19], the unscented Kalman filter [20] and the sliding mode observer [21], [22] were usually used to improve the performance of the sensorless control. Nevertheless, since a large amount of calculation were unavoidable in those control methods, they were not

The associate editor coordinating the review of this manuscript and approving it for publication was Zhuang Xu.

suitable for the long-distance auto-transportation system. Some scholars began to adopt the artificial intelligence algorithms to the sensorless control in order to get better control performance [23], [24], but this technology was not mature enough in the control engineering of the segmented PMLSM used in the long-distance auto-transportation system.

Moreover, due to the discontinuity of the stator part in the segmented PMLSM, the PM mover must pass different stator parts frequently. Owing to the assembly error between the segmented stator and the PM mover, the electromagnetic (EM) parameters of the segmented PMLSM are not constant values, so the precision of position estimation would be affected. Therefore, it is necessary to calibrate the EM parameters before the control model of the segmented PMLSM is switched from the normal control model into the sensorless control during the switch process. Many methods about the parameter calibration were used to justify the EM parameters of the segmented PMLSM. The least square method was proposed to calibrate the stator resistance and the synchronous inductance under the assumption that the permanent magnet (PM) flux linkage is constant [25], but it did not eliminate the influence of parameter variation on the identification precision. The parameter calibration was also realized by injecting the short-time alternating current (AC) disturbance [26], but the torque ripple was easily excited. An adaptive parameter identification algorithm based on an improved cooperative particle swarm optimization was used for the parameter identification [27]. Nevertheless, it was not suitable for the segmented PMLSM used in the long-distance auto-transportation system because of the high complexity and the extensive calculation. An online parameter identification method was proposed for the segmented PMLSM based on the real-time back EMF voltages and the speed of the PM mover, and it could quickly calibrate the flux linkages and the synchronous inductance before the PM mover entirely coincides with the stator part [28], so the EM parameters could be regulated in the sensorless control of the segmented PMLSM after the parameter calibration.

Above all, the position precision of the PM mover is distinctly affected by the variations of EM parameters because the PM mover and the segmented stators are not fixedly paired during the switch process. Therefore, the sensorless control is innovatively combined with the parameter calibration to reduce the influence of EM parameter variation on control performance in this article, and an improved integrator based on the model reference adaptive principle is used to improve the estimation precision and the robustness.

This article is organized as follows. In section II, the model of the segmented PMLSM is developed, and the influences of EM parameter variation on the sensorless control are analyzed. The specific principles of the parameter calibration and the sensorless control are designed in section III. The section IV introduces the simulation and experimental results to validate effectiveness of the proposed control method. Some essential conclusions are summarized in section V.

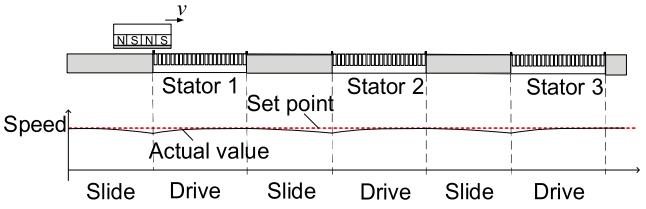

FIGURE 1. The diagram of the segmented PMLSM.

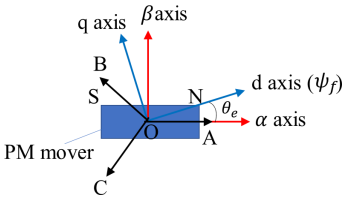

FIGURE 2. The coordinate system of the PM mover.

II. MODELING OF SEGMENTED PMLSM SYSTEM

The structure of the segmented PMLSM is shown in FIGURE 1, and it is consisted of the primary stator and the secondary PM mover. For the primary stator part, the stators with driving coils and the rails without driving coils are placed alternatively according to the length ratio. For the PM mover, there are three motion processes including the drive process, the switch process and the slide process. The PM mover is totally above the stator with driving coils during the drive process, and it would be accelerated to the rate speed. When one part of the PM mover is above the stator with driving coils and another part of the PM mover is on the rail without driving coils, the segmented PMLSM works at the switch process. The slide process happens when the PM mover entirely slides on the rail without driving coils. Each stator with driving coils has its independent drive module during the drive and switch process.

As like the rotary electric motor, the coordinate system of the PM mover in the segmented PMLSM could be presented in FIGURE 2. The voltage equations of the PM mover in $\alpha\beta$ axes are

$$\begin{cases} u_\alpha = R_s i_\alpha + L_\alpha \dfrac{di_\alpha}{dt} - \psi_f \dfrac{\pi v}{\tau} \sin\theta \\ u_\beta = R_s i_\beta + L_\beta \dfrac{di_\beta}{dt} + \psi_f \dfrac{\pi v}{\tau} \cos\theta \end{cases} \tag{1}$$

where u_α and u_β are stator voltages in $\alpha\beta$ axes, R_s is the stator resistance, i_α and i_β are stator currents in $\alpha\beta$ axes, L_α and L_β are inductances in $\alpha\beta$ axes, v is the speed of the PM mover, and τ is the pole pitch, and ψ_f is the PM flux linkage.

The flux linkage equations in $\alpha\beta$ axes could be written as

$$\begin{cases} \psi_\alpha = \int (u_\alpha - R_s i_\alpha) dt \\ \psi_\beta = \int \left(u_\beta - R_s i_\beta\right) dt \end{cases} \tag{2}$$

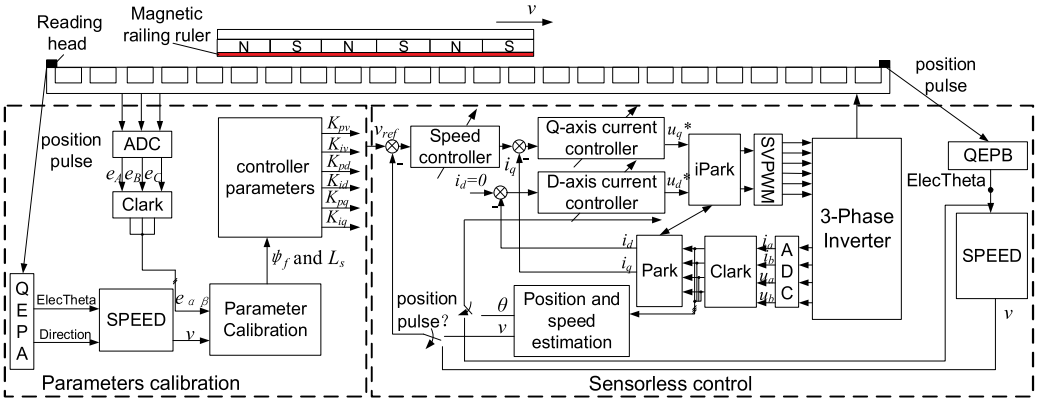

FIGURE 3. The control scheme of segmented PMLSM.

Combing (1) and (2), we could get

$$\begin{cases} \psi_\alpha = L_\alpha i_\alpha + \psi_f \dfrac{\pi v}{\tau} \cos\theta \\ \psi_\beta = L_\beta i_\beta + \psi_f \dfrac{\pi v}{\tau} \sin\theta \end{cases} \tag{3}$$

The basic integration equations of the speed and position are

$$\begin{cases} v = \dfrac{\tau}{\pi}\omega_r = \dfrac{\tau}{\pi}\dfrac{d\theta_r}{dt} \\ x = \displaystyle\int v dt = \frac{\tau}{\pi}\theta_r = \frac{\tau}{\pi}\text{actan}\frac{\psi_\beta - L_\beta i_\beta}{\psi_\alpha - L_\alpha i_\alpha} \end{cases} \tag{4}$$

where x is the estimated position of the PM mover, ψ_α and ψ_β are the flux linkages in $\alpha\beta$ axes. Therefore, the estimation accuracies of the position and speed are directly affected by the inductance and the flux linkage, so it is necessary to calibrate the EM parameters of the segmented PMLSM to tune control parameters during the switch process.

The whole control scheme of the segmented PMLSM is shown in FIGURE 3, there are two control loops including the speed control loop and the current control loop. For measurement system of the segmented PMLSM, the magnetic ruler is fixed at the bottom of the PM mover, and the reading heads at two ends of stator and rail could detect motion process of the PM mover, and then the parameter calibration is determined by the position signal captured by the reading heads. On the other hand, the control process of the PM mover has two parts including the parameter calibration module and the sensorless control module. When the PM mover enters the stator with driving coils, the speed of the PM mover is measured by the magnetic ruler, and the back EMF voltage and the electric angle are recorded by the current sampling circuit. Furthermore, the EM parameter calibration is conducted to calibrate the stator inductance and the flux linkage, and then the control parameters are regulated. The position pulse of the PM mover is captured when it completely coincides with the stator, and then the sensorless control method is applied. Moreover, the electric angle and the speed of the PM mover are estimated based on the d-axis current and the q-axis current, and then the estimated speed of the PM mover would be fed back to the speed control loop. The current control loop is realized based on the feedback current in dq axes and the input current through the speed control loop, and the input d-axis current is often defined as $i_d = 0$.

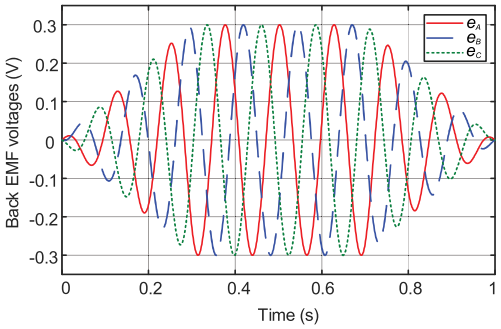

FIGURE 4. The back EMF voltages e_A, e_B, e_C.

III. ANALYSIS OF SENSORLESS CONTROL AND PARAMETER CALIBRATION

A. ANALYSIS OF PARAMETERS CALIBRATION

In general, the EM parameters of the PMLSM are considered as the constant values in the drive process and the switch process, so the control performance during the drive processes could not be maintained in the switch process. To improve the control performance of the sensorless control, the EM parameters should be calibrated when the PM mover enters a stator with driving coils from the rail. In detail, the synchronous inductance and the stator flux linkage could be estimated through the back EMF voltages of the segmented PMLSM, and then the control parameters could be updated in different motion process of the PM mover.

As shown in FIGURE 4, the back EMF voltages of the segmented PMLSM vary with the coupling area between the PM mover and the stator when the PM mover passes the stator at a constant speed, the back EMF voltage would increase with the coupling area during the drive process and the switch process. Therefore, the flux linkages of the segmented PMLSM could be achieved through the back EMF voltages.

According to the *Faraday's law* of electromagnetic induction, the back EMF voltages of the segmented PMLSM could be described as

$$\begin{cases} e_A = P\cos\theta \\ e_B = P\cos\left(\theta - \frac{2}{3}\pi\right) \\ e_C = P\cos\left(\theta + \frac{2}{3}\pi\right) \end{cases} \tag{5}$$

Furthermore, the e_α, e_β in the static coordinate could be obtained by the *Clark* transformation. Then, the amplitude P could be obtained by

$$P = \sqrt{e_\alpha^2 + e_\beta^2} \tag{6}$$

The PM flux linkage ψ_f could be calculated as

$$\psi_f = \frac{\tau}{\pi} e_0 v \tag{7}$$

where e_0 is no-load back EMF, and it could be achieved as

$$e_0 = \sqrt{3} E_0 \tag{8}$$

where $E_0 = P/\sqrt{2}$.

Therefore, the flux linkage ψ_f could be obtained by

$$\psi_f = \sqrt{\frac{3}{2}} \frac{P\tau}{\pi v} \tag{9}$$

Moreover, the PM flux linkage ψ_f is the product of the PM equivalent excitation inductance L_m and the PM equivalent current i_f, and the equivalent excitation inductance is

$$L_m = \frac{\psi_f}{i_f} \tag{10}$$

where $i_f = H_c/h_m$, and H_c is the coercivity of the PM mover, and h_m is the magnetism length of the PM mover.

Since the structure of the segmented PMLSM is surface-mounted type, the leakage inductance $L_{s\sigma}$ is a constant, and the synchronous inductance is

$$L_s = L_{s\sigma} + L_m \tag{11}$$

Therefore, the PM flux linkage ψ_f and the synchronous inductance L_s could be calibrated from (9) and (11). The control parameters K_{pv}, K_{iv} of the speed loop could be adjusted by

$$\begin{cases} K_{pv} = \dfrac{\beta M \tau}{1.5\pi P_n \psi_f} \\ K_{iv} = \beta K_{pv} \end{cases} \tag{12}$$

where β is the expected bandwidth of the speed loop, M is the mass of the PM mover, p_n is the pole of pairs.

For the current loop of the segmented PMSLM, the internal model control is used for the parameter adjustment, there are

$$\begin{cases} K_{pd} = \alpha L_d \\ K_{id} = \alpha R_s \\ K_{pq} = \alpha L_q \\ K_{iq} = \alpha R_s \end{cases} \tag{13}$$

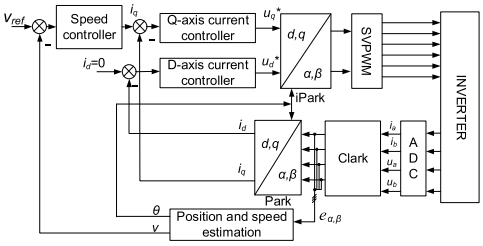

FIGURE 5. The diagram of the sensorless control method.

where α is the bandwidth of the current loop, and it could be achieved by

$$\alpha = \frac{2\pi}{T} = \max\left\{\frac{2\pi R}{L_d}, \frac{2\pi R}{L_q}\right\} \tag{14}$$

According to (12), (13) and (14), the control parameters are proportional to the PM flux linkage ψ_f and the synchronous inductance L_s. According to the calibration values of coupling area between the PM mover and the stator with driving coils, the ratio between the updating value and the previous value of EM parameters could be calculated. When the PM mover enters a new stator with driving coils again, the control parameters could be updated according to this ratio to enhance the control performance.

B. ANALYSIS OF SENSORLESS CONTROL

The EM parameters of the segmented PMLSM would be updated by the parameter calibration in FIGURE 5, and then the sensorless control would be applied to the speed control of the PM mover when it entirely coincides with the stator during the drive process. The back EMF integration is used to estimate the position and speed of the PM mover during the sensorless control. The stator flux linkages ψ_α and ψ_β could be obtained by integration of the back EMF voltage.

According to (4), the back EMF integration could directly calculate the position and speed of the PM mover. Nevertheless, the back EMF integration usually has an integral drift due to the direct current (DC) offset and the initial value, so the saturation of the back EMF integrator would happen [29]. Although the low-pass filter could solve this problem, it cannot eliminate the DC offset and the large phase shift. In this paper, an improved integration method as shown in FIGURE 6 [30], using an adaptive compensation model, is used in the back EMF integration to estimate the flux linkage, thereby to estimate the position and speed of the PM mover. Furthermore, the control parameters in the sensorless control process could be updated.

The flux linkage compensator could be obtained by

$$\psi_{cmp} = \left(K_p + K_i s\right) \frac{\psi_\alpha V_{EMF\alpha} + \psi_\beta V_{EMF\beta}}{|\psi|} \tag{15}$$

So, the stator flux linkages could be estimated and corrected adaptively by the fact that the nominal stator flux linkage should be utterly orthogonal to the back EMF voltage. When the DC offset and an initial value cause the defletion

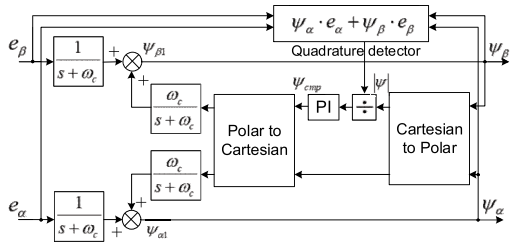

FIGURE 6. The diagram of the improved integrator.

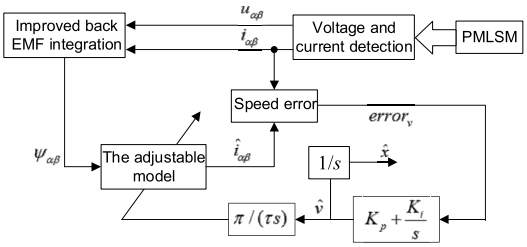

FIGURE 7. The block diagram of the improved integration method with the model reference adaptive algorithm.

of estimated stator flux linkage, the orthogonality would be affected immediately. In the meanwhile, a regulator could generate the compensation term of the orthogonality, and then it is fed back to the flux linkage estimation module. Consequently, the problems caused by the DC offset and the initial value could be solved.

In order to keep the stability of designed system, the model reference adaptive algorithm with the back-EMF integration is used to estimate the speed and position of the PM motor. The principle diagram is shown in FIGURE 7.

The flux linkage equations of the segmented PMLSM are

$$\begin{cases} \psi_\alpha = L_\alpha i_\alpha + \psi_f \cos\theta_r = |\psi_s| \cos\theta_r \\ \psi_\beta = L_\beta i_\beta + \psi_f \sin\theta_r = |\psi_s| \sin\theta_r \end{cases} \tag{16}$$

The control currents could be expressed into

$$\begin{cases} i_\alpha = \dfrac{\psi_\alpha}{L_\alpha} - \dfrac{\psi_f}{L_\alpha}\cos\theta_r = \dfrac{|\psi_s|}{L_\alpha}\cos\theta_r - \dfrac{\psi_f}{L_\alpha}\cos\theta_r \\ i_\beta = \dfrac{\psi_\beta}{L_\beta} - \dfrac{\psi_f}{L_\beta}\sin\theta_r = \dfrac{|\psi_s|}{L_\beta}\sin\theta_r - \dfrac{\psi_f}{L_\beta}\sin\theta_r \end{cases} \tag{17}$$

According to (16) and (17), there are

$$\begin{cases} \dfrac{di_\alpha}{dt} = -\dfrac{L_\beta}{L_\alpha}\omega_r i_\beta = -\dfrac{L_\beta}{L_\alpha}\dfrac{\pi}{\tau} v i_\beta \\ \dfrac{di_\beta}{dt} = \dfrac{L_\alpha}{L_\beta}\omega_r i_\alpha = \dfrac{L_\alpha}{L_\beta}\dfrac{\pi}{\tau} v i_\alpha \end{cases} \tag{18}$$

The state-space function could be written into

$$\begin{bmatrix} \dfrac{di_\alpha}{dt} \\ \dfrac{di_\beta}{dt} \end{bmatrix} = A \cdot \begin{bmatrix} i_\alpha \\ i_\beta \end{bmatrix} \tag{19}$$

And

$$A = \begin{bmatrix} 0 & -\dfrac{L_\beta}{L_\alpha}\dfrac{\pi}{\tau} v \\ \dfrac{L_\alpha}{L_\beta}\dfrac{\pi}{\tau} v & 0 \end{bmatrix} \tag{20}$$

According to the model reference adaptive principle, (18) could be used as an adjustable model with the adjustable parameter v, and the nominal model of the segmented PMLSM is used as the reference model.

The estimated form of (18) could be written into

$$\begin{cases} \dfrac{d\hat{i}_\alpha}{dt} = -\dfrac{L_\beta}{L_\alpha}\dfrac{\pi}{\tau}\hat{v}\hat{i}_\beta \\ \dfrac{d\hat{i}_\beta}{dt} = \dfrac{L_\alpha}{L_\beta}\dfrac{\pi}{\tau}\hat{v}\hat{i}_\alpha \end{cases} \tag{21}$$

The generalized error is defined as

$$e = i - \hat{i} \tag{22}$$

According to (18) and (21), the differential form of the error equation could be expressed as

$$\begin{bmatrix} \dfrac{de_\alpha}{dt} \\ \dfrac{de_\beta}{dt} \end{bmatrix} = A \cdot \begin{bmatrix} e_\alpha \\ e_\beta \end{bmatrix} - W\left(v - \hat{v}\right) J \begin{bmatrix} \hat{i}_\alpha \\ \hat{i}_\beta \end{bmatrix} \tag{23}$$

There are

$$\begin{cases} e_\alpha = i_\alpha - \hat{i}_a \\ e_\beta = i_\beta - \hat{i}_\beta \end{cases} \tag{24}$$

And

$$W = \left(v - \hat{v}\right) J \begin{bmatrix} \hat{i}_\alpha \\ \hat{i}_\beta \end{bmatrix} \tag{25}$$

It also could be expressed as the following form

$$\frac{de}{dt} = A \cdot e - W \tag{26}$$

To satisfy the *Popov* hyper-stable theory [31], the following two conditions must be satisfied.

1) The transfer matrix $H(s) = (sI - A_e)^{-1}$ must be a strictly positive definite matrix.

2) Given that γ_0 is a finite positive number, there is

$$\eta\left(0, t_1\right) = \int_0^t V^{\mathrm{T}} W dt > -\gamma_0^2, \quad \forall t_1 \geq 0 \tag{27}$$

According to (20), A_e satisfies the first condition. To satisfy the second condition, $\hat{v}$ is defined as

$$\hat{v} = \int_0^t \Phi_1\left(e, \tau, t\right) d\tau + \Phi_2\left(e, t\right) + \hat{v}\left(0\right) \tag{28}$$

Then $\eta(0, t_1)$ could be written as

$$\begin{aligned} &\eta\left(0, t_1\right) \\ &= \int_0^{t_1} e^T \left[\int_0^t \Phi_1\left(e, \tau, t\right) d\tau + \Phi_2\left(e, t\right) + \hat{v}\left(0\right) - v\right] J\hat{i} dt \\ &= \int_0^{t_1} e^T \left[\int_0^t \Phi_1\left(e, \tau, t\right) d\tau + \hat{v}\left(0\right) - v\right] J\hat{i} dt \end{aligned}$$

$$+\int_0^{t_1} e^T \Phi_2(e,t) J\hat{i} dt = \eta_1(0,t_1) + \eta_2(0,t_1) \quad (29)$$

For arbitrary functions, there is the following inequality

$$\eta(0,t_1) = \int_0^{t_1} kf(t) f'(t)\, dt = \frac{1}{2}k\left[f^2(t_1) - f^2(0)\right] > \frac{-1}{2}kf^2(0) = -\gamma_0^2 \quad (30)$$

There are assumptions as following

$$\begin{cases} f'(t) = e^T Ji \\ kf(t) = \int_0^t \Phi_1(e,\tau,t)\, d\tau + \hat{v}(0) - v \end{cases} \quad (31)$$

After the derivation, we could obtain

$$\begin{cases} \Phi_1(e,\tau,t) = K_i e^T J\hat{i}, & \text{if } K_i > 0 \\ \Phi_2(e,t) = K_p e^T J\hat{i}, & \text{if } K_p > 0 \end{cases} \quad (32)$$

where K_i and K_p are correlation coefficients.

There is

$$\eta_2(0,t_1) = K_p \int_0^{t_1} \left(e^T J\hat{i}\right)^2 dt \geq 0 \quad (33)$$

Therefore, the second condition is met by

$$\eta(0,t_1) = \eta_1(0,t_1) + \eta_2(0,t_1) \geq -\gamma_0^2 \quad (34)$$

According to (28) and (32), the adaptive law of speed could be described as

$$\begin{aligned} \hat{v} &= K_p e^T J\hat{i} + \int_0^t K_i e^T J\hat{i} d\tau + \hat{v}(0) \\ &= K_p\left[\frac{L_\alpha}{L_\beta}\frac{\pi}{\tau}\hat{i}_\alpha\left(i_\beta - \hat{i}_\beta\right) - \frac{L_\beta}{L_\alpha}\frac{\pi}{\tau}\hat{i}_\beta\left(i_\alpha - \hat{i}_\alpha\right)\right] \\ &\quad + \int_0^t\left[\frac{L_\alpha}{L_\beta}\frac{\pi}{\tau}\hat{i}_\alpha\left(i_\beta - \hat{i}_\beta\right) - \frac{L_\beta}{L_\alpha}\frac{\pi}{\tau}\hat{i}_\beta\left(i_\alpha - \hat{i}_\alpha\right)\right] d\tau \\ &\quad + \hat{v}(0) \end{aligned} \quad (35)$$

The estimated position could be achieved by integrating the speed of the PM mover

$$\hat{x} = \int_0^t \hat{v} d\tau \quad (36)$$

The control performance of the segmented PMLSM is improved by combining the parameters calibration with the improved back EMF integration method.

IV. SIMULATION AND EXPERIMENTS

A. SIMULATION RESULTS

In this part, simulations are conducted to verify the feasibility of the sensorless control with the parameter calibration, and the parameters of the segmented PMLSM used in simulations are listed in TABLE. 1.

TABLE 1. Parameters of simulation model.

Symbol	Parameter	Value
P_n	Pole of pairs	3
M	Mass of PM mover	5kg
B	Viscous friction factor	1.6
x_m	Length of PM mover	80mm
τ	Polar pitch	20mm
i_f	Equivalent current of PM	11A
$L_{s\sigma}$	Leakage inductance	2.8mH
ψ_f	PM flux linkage	0.02Wb
L_s	Synchronous inductance	4.6mH
v	Speed of PM mover	2m/s
	Length of each primary stator	400mm
	Distance of adjacent segments	100mm

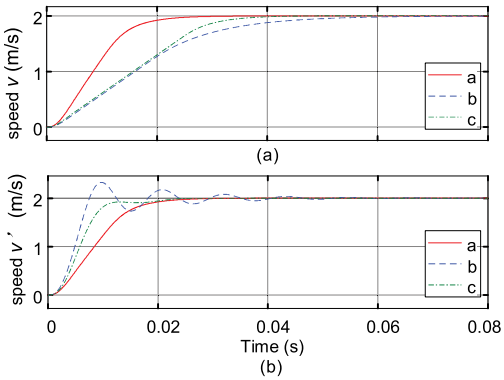

FIGURE 8. Speed response curves of the PM mover with different control models, (a) $\psi_f = 0.01$Wb and $L_s = 2.8$mH, (b) $\psi_f = 0.05$Wb and $L_s = 7.8$mH.

1) SIMULATION OF PARAMETER CALIBRATION

Two different groups (group A and group B) of simulations with different EM parameters are conducted to verify the effectiveness of the parameter calibration, and then three different control models (the nominal model, the perturbation model without the parameter calibration, the perturbation model with the parameter calibration) of the segmented PMLSM are analyzed and compared in each group as shown in FIGURE 8. The speed curve of the PM mover with the nominal model is shown by the red solid line (curve a), and that of the perturbation model without the parameter calibration is marked by the blue dashed line (curve b), finally the speed curve of the perturbation model with the parameter calibration is plotted by the green dotted line (curve c). In the group A, the PM flux linkage ψ_f is reduced from 0.02Wb to 0.01Wb, and the synchronous inductance L_s is declined from 4.6mH to 2.8mH, and the speed curves of the PM mover are plotted in FIGURE 8(a). There is no obvious difference on overshoot among three different control models, but the setting time of the perturbation model without the parameter calibration is about 0.06s and that of perturbation model with the parameter calibration is 0.04s, so the parameter calibration would improve the response speed of the segmented PMLSM. In the group B, the PM flux linkage sets at $\psi_f =$ 0.05Wb and the synchronous inductance $L_s = 7.8$mH. The

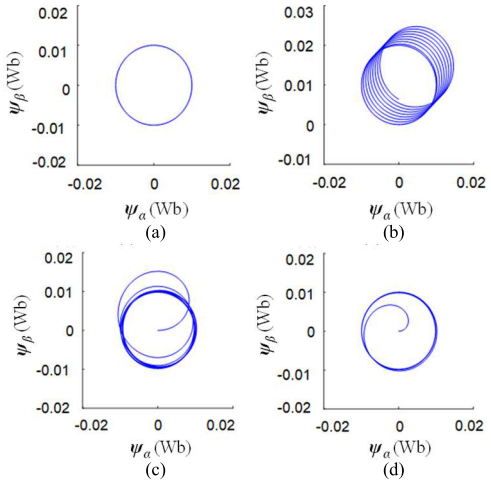

FIGURE 9. The trajectories of the stator flux linkages (ψ_α, ψ_β), (a) the reference flux linkage, (b) the flux linkage trajectory with a pure integrator, (c) the flux linkage with a low-pass filter, (d) the flux linkage with an improved integrator.

speed curves of three different control models are illustrated in FIGURE 8(b). The overshoot of the perturbation model without the parameter calibration reaches 15.2% and the setting time is 0.06s, but the perturbation model with the parameter calibration has no obvious overshoot and its setting time is 0.03s. Therefore, the control performances of simulation model with parameter calibration are better than that without parameter calibration by reducing the overshoot and the settling time, so it is necessary to calibrate the EM parameters when the PM mover runs on different stators during the switch process.

2) SIMULATION OF SENSORLESS CONTROL

In order to verify the effectivenss of the improved integrator used in the sensorless control, a DC offset with 0.05V is added to the back-EMF voltages e_α and e_β. The pure integrator, the low-pass filter and the improved integrator are respectively applied to estimate the stator flux linkages ψ_α and ψ_β, and the trajectories of the stator flux linkage are plotted in FIGURE 9. The reference flux linkage is a perfect cycle in FIGURE 9(a), and its radius is 0.01Wb. For the flux linkage with the pure integrator as shown in FIGURE 9(b), the deflection from reference flux linkage reaches to 0.015Wb. As illustrated in FIGURE 9(c), the flux linkage with the low-pass filter exceeds the radius of the reference flux linkage. Finally, the flux linkages with an improved integrator are close to the reference flux linkages in FIGURE 9(d). Therefore, the improved integrator could effectively restrain the DC offset and reduce the phase shift of flux linkage.

In addition, the position estimation accuracy of the improved integrator is also testified. The actual position of the PM mover is illuminated in FIGURE 10(a), and the estimated position of the PM mover applying the improved integrator is plotted in FIGURE 10(b). The error between the actual position and the estimated position is shown in FIGURE 10(c),

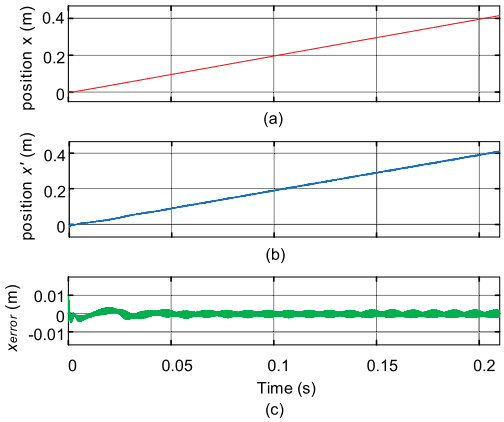

FIGURE 10. Comparison and error of the actual position and the estimated position of the PM mover, (a) the actual position, (b) the estimated position, (c) the position error.

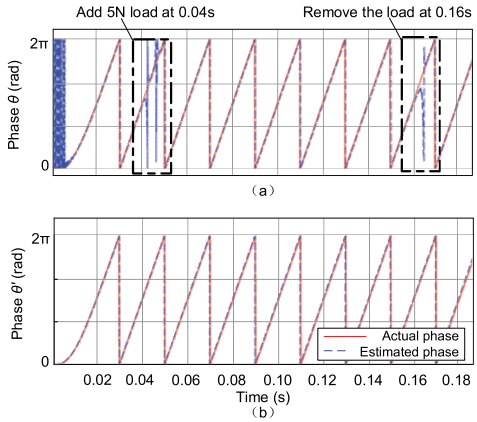

FIGURE 11. The phase comparisons of the back EMF voltages with two different methods, (a) phase comparison of the back EMF voltage with normal integrator, (b) phase comparison of the back-EMF with the improved integrator with the model reference adaptive principle.

and the estimation error approaches to a constant range within 0.002m. Therefore, the improved integrator used in the sensorless control of the segmented PMLSM could precisely track the actual position of the PM mover.

Furthermore, an improved integrator based on the model reference adaptive principle is used to improve the robustness of the segmented PMLSM. The phase of the back EMF voltage could be estimated by the model reference adaptive law, and the phase comparisons of the back EMF voltages with different control models are plotted in FIGURE 11 when the load disturbance is added on the PM mover at 0.04s and removed at 0.16s. The red solid line is the actual phase of the back EMF voltage, and the blue dotted line presents the estimated phase of the back EMF voltage. As shown in FIGURE 11(a), for the normal integration method used to estimate the back EMF voltage, there is an obvious phase jump when the load disturbance is imposed on the PM mover. For the improved integration method based on the model reference adaptive principle, the estimated phase of the back EMF voltage could accurately track the

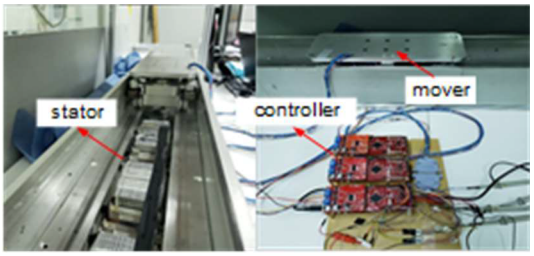

FIGURE 12. The experimental setup of the segmented PMLSM.

actual phase. Therefore, the improved integration method based on the model reference adaptive principle has strong anti-disturbance when the PM mover is suffered from disturbance.

B. EXPERIMENT RESULTS

Experiments are conducted to further prove the feasibility of the proposed control model for the segmented PMLSM. The experimental setup is shown in FIGURE 12, and it has two parts including the segmented PMLSM and the control system. For the control system, a digital signal processor (DSP) board (TMS320F28377s) is used as the main control unit (MCU) to realize the real-time control of the segmented PMLSM based on the position/speed signal captured by the magnetic rulers, and the control frequency is 10kHz. The driver board DRV8301 is used to drive the stator coils of the segmented PMSLM. During the experiment, the PM mover is driven to the reference speed using the sensorless control during the drive process, and the parameter calibration is conducted during the switch process to regulate the control parameters.

1) EXPERIMENT OF PARAMETERS CALIBRATION

Firstly, the effectiveness of the parameter calibration is verified through calibrating the back EMF voltage, the PM flux linkage and the synchronous inductance in the experiment. The calibrated results of the EM parameters are shown in FIGURE 13 when the PM mover works at the switch process from the rail without driving coils into the stator with driving coils. The nominal value of the PM flux linkage $\psi_f = 0.02$Wb and the synchronous inductance $L_s = 4$mH, respectively. As shown in FIGURE 13, the calibrated results of the EM parameters converge to the nominal values at 0.15s.The error between the calibrated result and the nominal value of the PM flux linkage is 0.001Wb in FIGURE 13(b), and the error of the synchronous inductance is 0.1mH as shown in FIGURE 13(c). Therefore, the parameter calibration could be used in the sensorless control of the segmented PMLSM to improve the estimation precision of the position and speed during the switch process.

2) EXPERIMENT OF SENSORLESS CONTROL

Moreover, as illustrated in FIGURE 14, the phases of the back EMF voltages are measured and compared in the experiment.

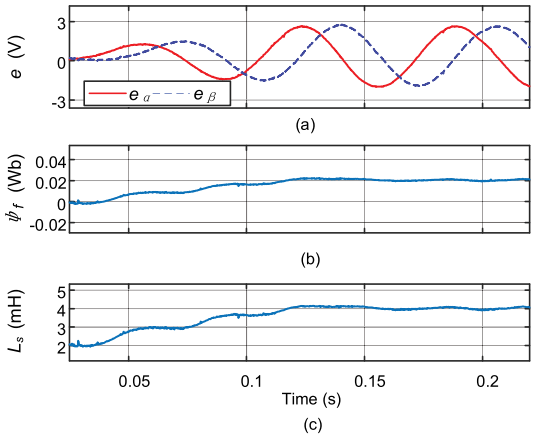

FIGURE 13. The calibration results of the EM parameters, (a) the back EMF voltages in $\alpha\beta$ axes, (b) the PM flux linkage, (c) the synchronous inductance.

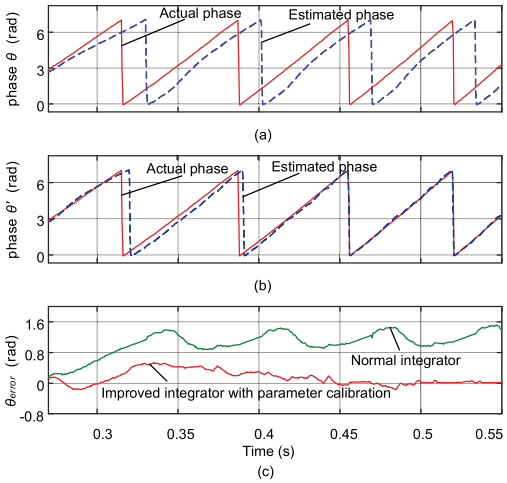

FIGURE 14. The actual and estimated phases of the back EMF voltages, (a) the actual and estimated phases of the back EMF with the normal integration method, (b) the actual and estimated phases of the back EMF with the improved integration method, (c) the comparison of estimated phase error of the back EMF voltage.

For the phase of the back EMF voltage estimated by the normal integration method in FIGURE 14(a), the error between the actual and estimated phases of the back EMF voltage reaches to 1.5rad, so there is obvious phase shift by using the normal integrator in the sensorless control. In addition, the phase of the back EMF voltage estimated by the improved integrator with the parameter calibration is plotted in FIGURE 14(b), the error between the actual phase and the estimated phase is declined from 1.5rad to 0.07rad. Therefore, the improved integration in the sesnorless control of the segmented PMLSM has better performance on estimating the back EMF voltage, and then control precision of the segmented PMLSM would be improved.

The speed curve of the PM mover is shown in FIGURE 15. The speed of the PM mover is 1.772m/s when it starts to enter the stator with driving coils from the rail without driving coils, and then the speed of the PM mover is accelerated to the rate

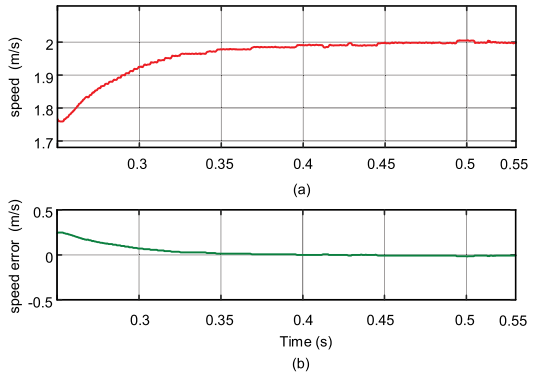

FIGURE 15. (a) The speed curve of the PM mover, (b) the error between the reference speed and the actual speed.

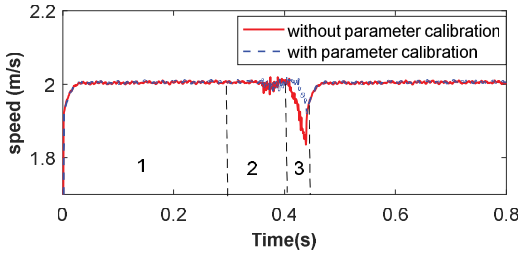

FIGURE 16. The speed curve of the PM mover during three motion processes.

speed (2m/s). At t = 0.45s, the actual speed of the PM mover converges to the rate value, and the error between the actual and the rate speed is restrained to 0.04m/s. Those results satisfy the requirements of the segmented PMLSM on speed convergence and stability. Furthermore, the speed curve of the PM mover during three motion processes is plotted in FIGURE 16, there are obvious oscillations during the swtich process and speed reduction during the slide process. For the speed curve of the PM mover without the parameter calibration shown by the red line, the speed of the PM mover would be reduced to 1.82m/s. The speed curve of the PM mover with the paramter calibration is marked by the blue line, and the speed is only declined to 1.9m/s. Therefore, the sensorless control with the parameter calibration has better dynamic performance on the speed control of the segmented PMLSM.

V. CONCLUSION

In this article, the sensorless control model with the paramter calibration is of great significance for the application of the segnmented PMLSM in the long-distance auto-transportation system. The PM mover and stators of the segmented PMLSM are not fixedly paired, so the performance of the sensorless control would be affected when the PM mover slides into a new stator with driving coils during the swtich process. Thus, the parameter calibration is applied to get the accurate EM parameters during the switch process of the PM mover. An model reference adaptive integrator could improve the precision of the sensorless control and the anti-disturbance performance. This proposed control model could be applied to the control engineering of PMLSM with segmented stators.

REFERENCES

[1] Q. Tan, X. Huang, L. Li, and M. Wang, "Research on inductance unbalance and thrust ripple suppression of slot-less tubular permanent magnet synchronous linear motor," *IEEE Access*, vol. 6, pp. 51011–51020, 2018.

[2] M. A. M. Cheema, J. E. Fletcher, D. Xiao, and M. F. Rahman, "A direct thrust control scheme for linear permanent magnet synchronous motor based on online duty ratio control," *IEEE Trans. Power Electron.*, vol. 31, no. 6, pp. 4416–4428, Jun. 2016.

[3] F. Song, Y. Liu, J.-X. Xu, X. Yang, P. He, and Z. Yang, "Iterative learning identification and compensation of space-periodic disturbance in PMLSM systems with time delay," *IEEE Trans. Ind. Electron.*, vol. 65, no. 9, pp. 7579–7589, Sep. 2018.

[4] T. Wen, B. Xiang, Z. Wang, and S. Zhang, "Speed control of segmented PMLSM based on improved SMC and speed compensation model," *Energies*, vol. 13, no. 4, p. 981, Feb. 2020.

[5] R. Hellinger and P. Mnich, "Linear motor-powered transportation: History, present status, and future outlook," *Proc. IEEE*, vol. 97, no. 11, pp. 1892–1900, Nov. 2009.

[6] J. Fang, D. B. Montgomery, and L. Roderick, "A novel MagPipe pipeline transportation system using linear motor drives," *Proc. IEEE*, vol. 97, no. 11, pp. 1848–1855, Nov. 2009.

[7] Y.-S. Huang and C.-C. Sung, "Function-based controller for linear motor control systems," *IEEE Trans. Ind. Electron.*, vol. 57, no. 3, pp. 1096–1105, Mar. 2010.

[8] C.-C. Sung and Y.-S. Huang, "Based on direct thrust control for linear synchronous motor systems," *IEEE Trans. Ind. Electron.*, vol. 56, no. 5, pp. 1629–1639, May 2009.

[9] K. Suzuki, Y.-J. Kim, and H. Dohmeki, "Proposal of the long-distance transportation system in the factory using PM-LSM," in *Proc. Int. Conf. Elect. Mach. Syst.*, 2009, pp. 1–6.

[10] Y. J. Kim and H. Dohmeki, "Driving method of stationary discontinuous-armature PMLSM by open-loop control for stable-deceleration driving," *IET Electr. Power Appl.*, vol. 1, no. 2, pp. 248–254, Mar. 2007.

[11] D. Hall, J. Kapinski, M. Krefta, and O. Christianson, "Transient electromechanical modeling for short secondary linear induction machines," *IEEE Trans. Energy Convers.*, vol. 23, no. 3, pp. 789–795, Sep. 2008.

[12] K. Suzuki, Y.-J. Kim, and H. Dohmeki, "Driving method of permanent-magnet linear synchronous motor with the stationary discontinuous armature for long-distance transportation system," *IEEE Trans. Ind. Electron.*, vol. 59, no. 5, pp. 2227–2235, May 2012.

[13] M. A. M. Cheema, J. E. Fletcher, M. Farshadnia, D. Xiao, and M. F. Rahman, "Combined speed and direct thrust force control of linear permanent-magnet synchronous motors with sensorless speed estimation using a sliding-mode control with integral action," *IEEE Trans. Ind. Electron.*, vol. 64, no. 5, pp. 3489–3501, May 2017.

[14] L. Li, H. Zhu, M. Ma, and Q. Chen, "Proposal of the sensorless control method of long primary segmented PMLSM applied in electromagnetic catapult," in *Proc. 16th Int. Symp. Electromagn. Launch Technol.*, 2012, pp. 1–6.

[15] C. Yang, T. Ma, Z. Che, and L. Zhou, "An adaptive-gain sliding mode observer for sensorless control of permanent magnet linear synchronous motors," *IEEE Access*, vol. 6, pp. 3469–3478, 2018.

[16] M. Seilmeier and B. Piepenbreier, "Sensorless control of PMSM for the whole speed range using two-degree-of-freedom current control and HF test current injection for low-speed range," *IEEE Trans. Power Electron.*, vol. 30, no. 8, pp. 4394–4403, Aug. 2015.

[17] K. Urbanski, "Sensorless control of PMSM at low speed range using reference model," in *Proc. 17th Eur. Conf. Power Electron. Appl. (EPE ECCE-Europe)*, 2015, pp. 1–8.

[18] P. Du, Z. Guan, T. Wang, and Y. Zhang, "Operation research on two kinds of high-frequency signal injection method combined with coordinate system," *Electr. Mach. Control Appl.*, no. 2, p. 6, 2017.

[19] L. Saihi, A. Bouhenna, M. Chenafa, and A. Mansouri, "A robust sensorless SMC of PMSM based on sliding mode observer and extended Kalman filter," in *Proc. 4th Int. Conf. Elect. Eng. (ICEE)*, 2015, pp. 1–4.

[20] D. Janiszewski, "Sensorless control of permanent magnet synchronous motor based on unscented Kalman filter," in *Proc. Int. Conf. Power Eng., Energy Elect. Drives*, 2011, pp. 1–6.

[21] W.-C. Chi, M.-Y. Cheng, and C.-H. Chen, "Position-sensorless method for electric braking commutation of brushless DC machines," *IET Electr. Power Appl.*, vol. 7, no. 9, pp. 701–713, Nov. 2013.
[22] H. Lu, J. Wu, and M. Li, "A new sliding mode observer for the sensorless control of a PMLSM," in *Proc. 29th Chin. Control Decis. Conf. (CCDC)*, 2017, pp. 5364–5369.
[23] H. Jin and X. Zhao, "Complementary sliding mode control via elman neural network for permanent magnet linear servo system," *IEEE Access*, vol. 7, pp. 82183–82193, 2019.
[24] M. Niaz Azari, M. Mirsalim, S. M. Abedi Pahnehkolaei, and S. Mohammadi, "Optimum design of a line-start permanent-magnet motor with slotted solid rotor using neural network and imperialist competitive algorithm," *IET Electr. Power Appl.*, vol. 11, no. 1, pp. 1–8, Jan. 2017.
[25] S. Ichikawa, M. Tomita, S. Doki, and S. Okuma, "Sensorless control of permanent-magnet synchronous motors using online parameter identification based on system identification theory," *IEEE Trans. Ind. Electron.*, vol. 53, no. 2, pp. 363–372, Apr. 2006.
[26] H. Wang, Y.-C. Liu, and X. Ge, "Sliding-mode observer-based speed-sensorless vector control of linear induction motor with a parallel secondary resistance online identification," *IET Electr. Power Appl.*, vol. 12, no. 8, pp. 1215–1224, Sep. 2018.
[27] Z.-H. Liu, J. Zhang, X.-H. Li, and Y.-J. Zhang, "Immune co-evolution particle swarm optimization for permanent magnet synchronous motor parameter identification," *Acta Automatica Sinica*, vol. 38, no. 10, p. 1698, 2012.
[28] J. Wang, L. Gao, and Z. Lin, "Adaptive on-line Identification Method for Parameters of Permanent Magnet Synchronous Motor," *Micromotors*, vol. 48, no. 12, pp. 79–83, 2015.
[29] C. Xia, Y. Yan, B. Ji, and T. Shi, "Two-degree-of-freedom proportional integral speed control of electrical drives with Kalman-filter-based speed estimation," *IET Electr. Power Appl.*, vol. 10, no. 1, pp. 18–24, Jan. 2016.
[30] J. Hu and B. Wu, "New integration algorithms for estimating motor flux over a wide speed range," *IEEE Trans. Power Electron.*, vol. 13, no. 5, pp. 969–977, Sep. 1998.
[31] J. Choi, K. Nam, A. A. Bobtsov, A. Pyrkin, and R. Ortega, "Robust adaptive sensorless control for permanent-magnet synchronous motors," *IEEE Trans. Power Electron.*, vol. 32, no. 5, pp. 3989–3997, May 2017.

TONG WEN was born in Hunan, in 1983. He received the B.S. and Ph.D. degrees from the Beijing University of Aeronautics and Astronautics, Beijing, China, in 2005 and 2012, respectively. He is currently a Lecturer and a master's Tutor with the School of Instrumentation and Optoelectronic Engineering, Beihang University. His current research interests include linear motor control, control of the active magnetic bearing, and magnetic suspension inertial stabilization platform used in the aviation remote sensing systems.

ZHONGYI WANG was born in Shandong. She received the B.S. degree from Guangxi University, Nanning, China, in 2018. She is currently pursuing the degree with the School of Instrumentation and Optoelectronic Engineering, Beihang University, Beijing, China. Her research interest includes motor control.

BIAO XIANG was born in 1987. He received the B.S. degree in physical and mechanical and electrical engineering from Xiamen University, Xiamen, China, and the M.S. degree in instrumentation science and opto-electronics engineering from Beihang University (Beijing University of Aeronautics and Astronautics), Beijing, China. He is currently pursuing the Ph.D. degree in vibration analysis and control with the Department of Mechanical Engineering, The Hong Kong Polytechnic University, Hong Kong. His research interests include vibration measurement analysis, active vibration control, and control of magnetically suspended rotational machines.

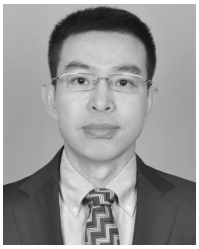

BANGCHENG HAN (Member, IEEE) was born in 1974. He received the M.S. degree in mechanical design and theory from Jilin University, Changchun, China, in 2001, and the Ph.D. degree in mechanical manufacture and automation from the Changchun Institute of Optics, Fine Mechanics and Physics, Chinese Academy of Sciences, Changchun, in 2004. He is currently a Professor with the School of Instrumentation and Optoelectronic Engineering, Beihang University, Beijing, China. His research interests include mechatronics, magnetic suspension technology, and attitude control actuator of spacecraft.

HAITAO LI (Member, IEEE) was born in Shandong, in 1979. He received the B.S. and M.S degrees from Shandong University, Jinan, China, in 2002 and 2005, respectively, and the Ph.D. degree from the Beijing University of Aeronautics and Astronautics, Beijing, China, in 2009. He is currently an Associate Professor with the School of Instrumentation and Optoelectronic Engineering, Beihang University. He is also with the Fundamental Science on Novel Inertial Instrument and Navigation System Technology Laboratory, China. His main research interest includes magnetically suspended control moment gyro (MSCMG) and its nonlinear control.